Chapter 5

Statistics of Subsurface Kinetic Helicity in Active Regions

5.1 Introduction

Observations have revealed that a hemispheric preference of magnetic chirality (handedness) exists throughout the solar atmosphere. Pevtsov, Canfield, & Metcalf (1995) used photospheric vector magnetograms of active regions from Mees Solar Observatory to compute the linear force-free field α-coefficient, and they found among 69 active regions studied α was negative (positive) in 69% (75%) of northern (southern) hemisphere active regions. Later analysis of more active regions showed similar results (Longcope, Fisher, & Pevtsov, 1998). Bao & Zhang (1998) used vector magnetograms from Huairou Solar Observing Station to compute current helicity density h_c of 422 active regions, and found that 84% (79%) of active regions in northern (southern) hemisphere had negative (positive) h_c. It was found more recently that α-coefficient and h_c for active regions in Solar Cycle 23 retain a similar hemispheric preference as in Solar Cycle 22 (Pevtsov, Canfield, & Latushko, 2001).

Besides statistical work on vector magnetograms, statistics were also done on the shapes of sigmoidal coronal loops. Canfield & Pevtsov (1999) studied X-ray images from the *Yohkoh* soft X-ray telescope, and found that 59% (68%) of sigmoidal coronal loops displayed an inverse-S (S) shape in the northern (southern) hemisphere.

Hα analysis of solar filaments in the chromosphere gave similar results (Pevtsov, Balasubramaniam, & Rogers, 2003).

Several mechanisms have been proposed to explain the observed hemispheric preference, such as differential rotation (e.g., DeVore, 2000), dynamo models (Gilman & Charbonneau, 1999), and the non-vanishing kinetic helicity $\langle \mathbf{v} \cdot (\nabla \times \mathbf{v}) \rangle$ (here and after, $\langle\rangle$ means to compute the average, and $\mathbf{v}$ is velocity) in the turbulent convection zone (Longcope, Fisher, & Pevtsov, 1998). Although most work agrees that the formation of the magnetic chirality results from the kinetic helicity, no statistical work has been able to be performed so far to study the kinetic helicity in the solar photosphere and subphotospheric regions.

In the last two chapters, I have shown that time-distance measurement and its inversion can reveal the three-dimensional subsurface flow maps in active regions to a depth of approximately 12 Mm, which enables the computation of subsurface kinetic helicity. Therefore, a statistical study of subsurface kinetic helicity in solar active regions is feasible to investigate the relationship between subphotospheric kinetic helicity and photospheric magnetic helicity. Furthermore, it is also of great help in understanding the physical conditions in the convection zone and testing solar dynamo models.

In this chapter, I apply our time-distance technique on 88 sets of active region data taken between 1997 to 2002 by the MDI mission to infer their subsurface flow fields and compute the average subsurface kinetic helicity. The statistical results on the latitudinal distribution of kinetic helicity, relationship of kinetic helicity and magnetic strength are presented in this chapter.

5.2 Observations and Data Reduction

SOHO/MDI had around 2 months of dynamic campaign data each year from 1996 to the present, and provided nearly uninterrupted one minute cadence Dopplergrams, which are valuable to perform helioseismology studies. From these dynamic periods from 1997 to 2002 and a few other continuous coverage periods, we have chosen 77 active regions, and performed 88 sets of time-distance computations, with 9 active regions computed in two different time periods, and 1 active region computed in three periods.

For all the 88 sets of data, we derived three-dimensional subsurface velocity fields, from which we then computed kinetic helicity $\alpha_v = \mathbf{v} \cdot (\nabla \times \mathbf{v})$. However, we adopted only the vertical component $\alpha_v^z = v_z(\partial v_y/\partial x - \partial v_x/\partial y)$ for computation, so that we can avoid the derivatives in vertical (z) direction where we have only a few layers. In addition, we can keep accordance with previous studies of current helicity, in which only the vertical component of current helicity was derived. Before computing the kinetic helicity, we removed the differential rotation from each set of data in order to exclude the vorticity caused by rotation. After computing the α_v^z values at each pixel in the selected active regions, we averaged all α_v^z where the magnitude of line-of-sight magnetic field is larger than 100 Gauss to obtain a mean value of kinetic helicity of this active region, although the selection of 100 Gauss is arbitrary. All the detailed information of the active regions and results of the averaged kinetic helicity are presented in Table 5.1 for the northern hemisphere and Table 5.2 for the southern hemisphere. In the tables, $\langle\alpha_{v1}\rangle$ and $\langle\alpha_{v2}\rangle$ represent the mean kinetic helicity at $0-3$ Mm and $9-12$ Mm, respectively. $\langle|\mathbf{B}|\rangle$ represents the mean magnetic field strength for each active region, and $\langle|\alpha_{v1}|\rangle, \langle|\alpha_{v2}|\rangle$ represent the mean magnitude of kinetic helicity at different depths.

Some previous authors (e.g., Pevtsov, Canfield, & Metcalf, 1995) estimated the errors of mean α-coefficient or current helicity by computing the same active regions a few times at different observation time. However, considering the observational requirements for time-distance studies (512 minutes uninterrupted observation with one minute cadence) and the heavy computational burden, it is not easy for us to estimate the errors of the kinetic helicity mean values by means of repeated computations of one active region at different observation times. Instead, we divide the active regions randomly into two equal halves, and compute the mean kinetic helicity separately for these two half regions, hence to estimate the errors of the mean kinetic helicity in one active region.

AR number	Date (mm.dd.yyyy)	Latitude (degree)	$\langle\alpha_{v1}\rangle$ (10^{-3}ms^{-2})	$\langle\alpha_{v2}\rangle$ (10^{-3}ms^{-2})	$\lvert\langle\mathbf{B}\rangle\rvert$ (Gs)	$\langle\lvert\alpha_{v1}\rvert\rangle$ (10^{-3}ms^{-2})	$\langle\lvert\alpha_{v2}\rvert\rangle$ (10^{-3}ms^{-2})
8036	04.26.1997	18.68	0.0064	0.30	167	1.18	3.84
8038	05.11.1997	20.48	0.24	0.24	419	3.51	7.63
8040	05.20.1997	5.17	0.039	-0.13	292	1.81	7.19
8040	05.22.1997	5.07	0.23	-0.28	292	2.36	5.68
8045	-	1.50	0.0098	5.65	237	0.56	7.80
8052	06.16.1997	18.00	0.16	-0.72	237	1.47	5.27
8071	08.11.1997	25.45	0.0032	1.90	193	1.30	4.35
8117	12.12.1997	30.36	-0.60	-2.57	314	3.09	6.23
8535	05.12.1999	21.67	0.086	0.52	275	2.10	8.43
8541	-	21.01	0.0093	1.95	250	2.58	14.92
8545	05.20.1999	36.58	0.59	-2.63	277	2.92	9.81
8552	05.28.1999	18.48	-0.0071	-1.03	300	2.06	7.30
8555	-	19.55	0.33	1.71	260	2.36	14.12
8582	06.16.1999	26.47	0.0073	0.69	282	3.61	6.68
8990	05.12.2000	13.83	0.16	-2.16	354	3.62	13.36
8994	-	17.05	-0.35	0.19	412	6.06	10.17
9002	05.20.2000	18.88	0.30	0.0046	405	4.75	10.81
9002	05.22.2000	18.88	0.59	1.37	357	3.44	8.51
9004	05.20.2000	10.90	0.36	0.23	479	7.26	11.86
9004	05.22.2000	10.90	0.18	1.86	351	4.56	11.56
9026	06.07.2000	21.02	-0.064	-1.19	296	2.72	6.33
9030	-	19.24	0.35	-7.59	475	5.66	10.97
9033	06.12.2000	22.40	-0.20	0.12	298	2.51	10.05
9039	-	6.69	-0.24	-1.22	334	1.92	7.69
9041	-	16.45	0.53	-0.14	301	2.27	7.66
9055	06.27.2000	20.12	0.20	-3.89	417	4.38	7.44
9057	-	14.05	-0.32	-3.36	538	6.88	14.4
9070	07.07.2000	18.71	-0.04	-0.75	315	2.46	6.58
9114	08.07.2000	9.41	-0.39	-2.53	363	5.61	8.79
9114	08.08.2000	9.41	-0.94	-6.76	372	4.84	11.78
9115	-	17.14	0.85	1.61	377	5.00	6.98
9236	11.23.2000	19.82	0.70	2.93	420	5.01	19.28
9236	11.24.2000	19.82	0.23	-1.62	404	5.61	17.86
9387	03.25.2001	8.71	0.32	2.43	280	2.22	8.42
9393	03.29.2001	17.43	-0.38	-0.89	432	5.59	12.21
9406	04.01.2001	25.78	0.029	-1.53	277	3.54	10.33
9407	-	11.03	0.13	3.31	308	2.36	8.74
9418	04.09.2001	20.83	-0.23	-0.99	270	2.91	9.43
9433	04.24.2001	16.71	0.063	-0.57	317	3.96	8.08
9450	05.12.2001	5.81	0.49	2.63	334	2.21	5.83
9450	05.14.2001	5.81	0.18	1.99	256	1.68	5.64
9454	-	13.00	-0.36	2.63	298	3.58	8.87
9463	05.23.2001	7.60	0.024	0.14	371	4.09	8.77
9691	11.14.2001	8.33	-0.76	10.33	437	4.80	27.55
9694	-	13.81	-1.05	1.09	328	4.17	14.58

Table 5.1: Summary of data for the analyzed active regions in the northern hemisphere.

AR number	Date (mm.dd.yyyy)	Latitude (degree)	$\langle\alpha_{v1}\rangle$ (10^{-3}ms^{-2})	$\langle\alpha_{v2}\rangle$ (10^{-3}ms^{-2})	$\lvert\langle\mathbf{B}\rangle\rvert$ (Gs)	$\langle\lvert\alpha_{v1}\rvert\rangle$ (10^{-3}ms^{-2})	$\langle\lvert\alpha_{v2}\rvert\rangle$ (10^{-3}ms^{-2})
8035	04.26.1997	34.50	0.0013	-1.02	132	0.42	3.36
8048	06.03.1997	28.29	0.21	-1.07	303	3.78	8.51
8070	08.11.1997	19.52	-0.18	-0.85	183	1.14	4.83
8118	12.12.1997	39.69	-1.02	-0.44	257	2.60	10.11
8120	-	22.31	-0.31	-1.03	197	0.74	6.00
8131	01.13.1998	22.48	-0.63	0.81	331	3.18	5.68
8143	01.29.1998	35.71	-0.034	-0.079	287	3.23	7.06
8156	02.16.1998	24.78	-0.19	1.34	410	4.00	11.08
8158	-	22.87	0.091	-2.73	242	1.39	16.50
8534	05.12.1999	24.19	0.10	-0.75	246	1.21	5.87
8540	-	17.29	-0.54	-0.65	316	2.57	4.63
8542	05.20.1999	21.07	-0.66	-0.47	331	2.61	7.96
8544	-	18.69	-0.45	-2.22	260	2.16	6.13
8583	06.16.1999	19.50	-0.26	-1.33	275	2.90	10.00
8906	03.13.2000	20.71	0.17	-1.56	310	2.30	6.53
8906	03.14.2000	20.71	-0.20	-0.17	317	3.15	7.11
8907	03.12.2000	16.83	-0.38	-2.61	410	5.39	22.08
8907	03.13.2000	16.83	-0.46	2.65	449	5.25	17.92
8907	03.14.2000	16.83	0.53	-8.89	449	8.92	36.96
8993	05.12.2000	23.10	-0.38	0.17	331	3.73	5.52
8996	05.20.2000	20.78	-0.081	0.75	318	4.39	8.50
8998	-	12.22	-0.16	-0.63	351	4.03	14.20
9056	06.27.2000	13.09	0.25	0.92	464	4.96	7.68
9067	07.07.2000	19.62	-0.31	-1.07	466	6.60	7.72
9068	-	17.48	0.22	0.22	298	2.56	13.77
9389	03.25.2001	12.78	-0.24	0.21	258	2.12	6.87
9395	03.29.2001	9.05	-0.079	1.32	306	3.33	10.99
9396	03.25.2001	5.81	-0.29	0.16	256	1.37	7.15
9397	03.29.2001	9.03	0.051	-3.05	308	3.20	14.39
9404	04.01.2001	5.62	0.16	-0.83	306	2.65	6.45
9408	-	9.19	0.95	0.14	487	6.51	7.97
9417	04.07.2001	8.62	0.85	1.01	368	4.04	10.89
9415	-	21.47	0.13	1.34	384	4.57	22.65
9415	04.09.2001	21.47	-0.14	4.35	392	3.47	14.85
9435	04.24.2001	20.05	-0.77	-0.77	341	3.79	6.69
9451	05.12.2001	20.67	0.063	1.48	289	1.74	9.41
9452	-	17.00	-0.065	2.05	352	2.91	5.32
9455	-	17.71	0.10	0.0081	313	2.74	5.74
9690	11.14.2001	17.17	0.43	-0.17	336	4.44	7.31
9787	01.24.2002	8.17	-0.72	-4.48	375	5.51	12.38
9787	-	8.17	0.42	0.11	370	5.80	9.72
9802	02.01.2002	13.26	0.89	2.09	409	5.84	9.19
9856	03.10.2002	3.93	-1.57	-1.34	462	6.30	10.11

Table 5.2: Summary of data for the analyzed active regions in the southern hemisphere.

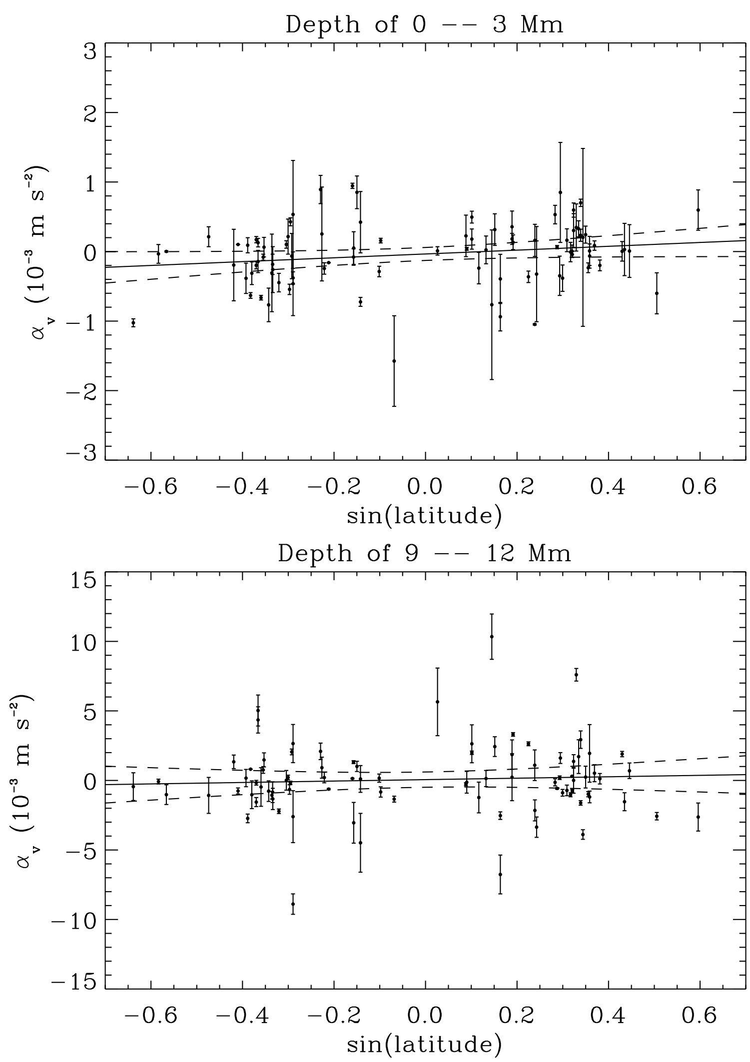

Figure 5.1: Latitudinal distribution of average kinetic helicity (α_v) from the selected active regions at two different depth intervals. The solid line in each panel is a linear fit to the scatter plot; the dashed lines indicate the 2σ error level of the fit (or 95% confidence level).

5.3 Statistical Results

5.3.1 Mean Kinetic Helicity vs Latitude

Figure 5.1 presents the latitudinal distribution of mean kinetic helicity for 88 sets of data at two different depth intervals 0 – 3 Mm and 9 – 12 Mm. It is found that at the depth of 0 – 3 Mm, among 45 active regions in the northern hemisphere, 30 (66.7%) have positive mean kinetic helicity, and among 43 active regions in the southern hemisphere, 25 (58.1%) have negative signs of mean kinetic helicity. A linear fitting of the latitudinal distribution was performed by use of the least squares. The dashed curve in the graph shows 2σ errors (i.e., 95% confidence level) of the mean kinetic helicity distribution, from which we can find that the mean kinetic helicity of the active regions is preferentially negative in the southern hemisphere and positive in the northern hemisphere. The percentage of dominant signs in each hemisphere is similar to the percentage in the coronal loop study by Canfield & Pevtsov (1999).

At the depth of 9 – 12 Mm, it is found that 25 (55.6%) active regions in the northern hemisphere have $\alpha_v^z > 0$, and 24 (55.8%) active regions in the southern hemisphere have $\alpha_v^z < 0$. The statistical percentages from both hemispheres only show a very weak hemispheric preference of the signs of kinetic helicity, while the linear fit and the 95% confidence band do not show clear evidence of this tendency.

5.3.2 Kinetic Helicity vs Magnetic Strength

It is generally believed that the solar magnetic field is produced by the solar dynamo at the base of the convection zone, and the poloidal field is produced by the toroidal field through α-effect, where α is proportional to the kinetic helicity $\langle \mathbf{v} \cdot (\nabla \times \mathbf{v}) \rangle$ through the solar convection zone (e.g., Gilman & Charbonneau, 1999). Therefore, since we have estimated the kinetic helicity in the active regions, it is of great interest to find whether there is any relationship between the magnetic field strength and the kinetic helicity.

Here, we average the magnitude of the kinetic helicity as $\langle |\alpha_v| \rangle$ over the areas where the magnetic strength is larger than 100 Gauss. The mean magnetic field strength $\langle |\mathbf{B}| \rangle$ for each active region is obtained by averaging the line-of-sight magnetic field strength in the same areas where the mean magnitude of kinetic helicity is obtained. Note that these two quantities are both from the average of the magnitudes regardless of the signs of the quantities.

Figure 5.2 shows scatter plots of the mean magnitude of the kinetic helicity versus

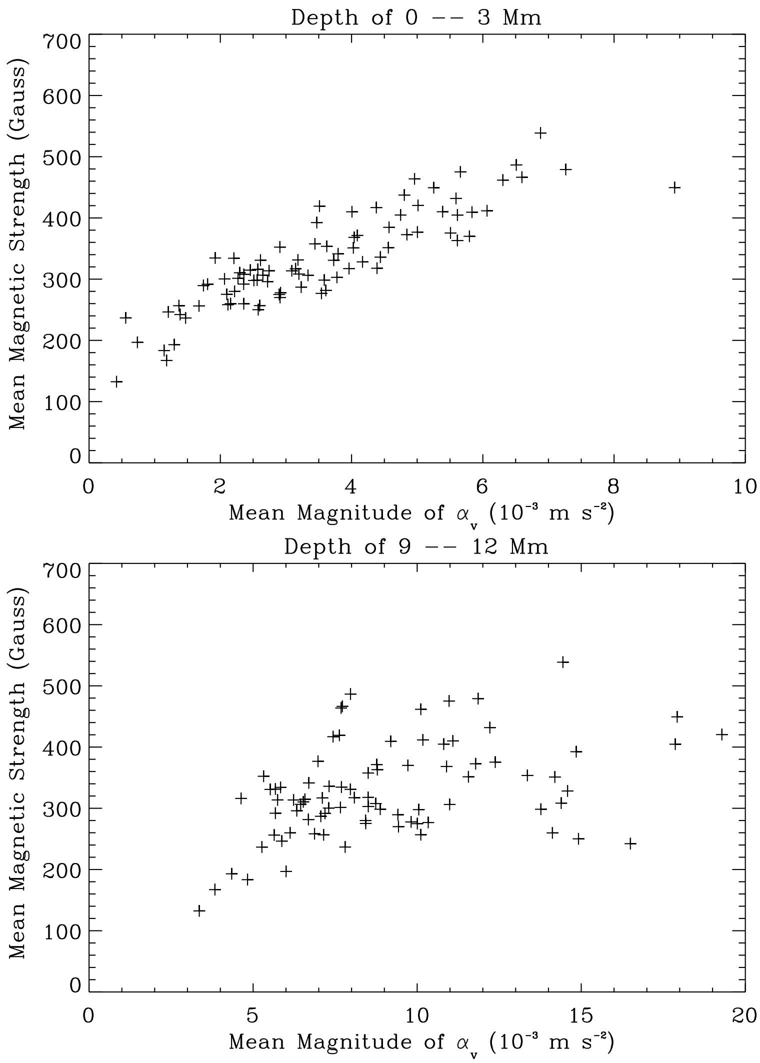

Figure 5.2: Scatter plot of the mean magnetic strength as a function of mean magnitude of kinetic helicity (α_v) from each selected active region.

the mean magnetic strength in all the 88 selected solar active region datasets. At the depth of 0 – 3 Mm, it shows that the mean magnetic strength seems linearly proportional to the mean magnitude of kinetic helicity, although the exact analytical relation is not clear. At the depth of 9 – 12 Mm, no obvious relation can be found between these two quantities, but it is basically true that the mean magnetic strength increases with the increase of the mean magnitude of kinetic helicity.

5.4 Discussion

Applying time-distance measurements and inversions on continuous Dopplergram observations has enabled us to detect the dynamics beneath the visible surface of active regions. The statistics of 88 active region datasets of Solar Cycle 23 show that at the depth of 0 – 3 Mm and 9 – 12 Mm, the distribution of mean kinetic helicity in active regions has a very slight hemispheric preponderance: negative in the southern hemisphere and positive in the northern hemisphere. Although the selection of 100 Gauss in the active regions as a computation criterion is arbitrary, the computations with 50 and 200 Gauss as criteria give us similar latitudinal distributions.

In Chapter 4, we have shown that the inversion technique applied to time-distance measurement could satisfactorily invert the vortical flows up to 12 Mm beneath the surface. But presumably the signals from time-distance measurements are becoming weaker with the increase of the depth, and how sensitive the time-distance measurements are to deep vortical flows is currently not known. So it is possible that some vortical flows may not be fully inverted and are underestimated. In addition, since we have little knowledge of the magnetic structures at the depth of 9 – 12 Mm, the selection of the computed region according to the photospheric magnetic field may be inaccurate. Particularly, at a few megameters beneath the surface, the velocity fields often extend to an area that is much larger than the surface structure (see figures in Chapter 3). Therefore, due to the above reasons, we may have underestimated the mean kinetic helicity at the depth of 9 – 12 Mm.

Overall, we find in our data that in the upper convection zone very close to the photosphere, kinetic helicity in active regions is slightly dominated by the positive sign in the northern hemisphere, and by the negative sign in the southern hemisphere. Therefore, the kinetic helicity preference has the opposite signs to the current helicity (or force-free coefficient α), which is negative (positive) in northern (southern) hemisphere. By simulating three-dimensional turbulent cyclonic magneto-convection, Brandenburg et al. (1990) found that in the upper layers of their magneto-convection model, the signs of kinetic helicity are opposite to the signs of the current helicity. In the more recent simulations of α-effect due to magnetic buoyancy as well as global rotation, Brandenburg & Schmitt (1998) confirmed the finding of opposite signs between kinetic helicity and current helicity, and furthermore they showed that the kinetic helicity in the northern hemisphere is positive. Later analytical analysis on the compressible turbulent field (Rüdiger, Pipin, & Belvedère, 2001) confirmed the results from the numerical simulations. Our observations of positive kinetic helicity in the northern hemisphere give the same sign as expected from these theoretical works. On the other hand, we must be aware of the high fluctuation shown in our results. It is also noticed that in numerical simulation of Brandenburg & Schmitt (1998), the kinetic helicity is also highly noisy and a positive sign of kinetic helicity could only be found with some cautious analysis.

It was recognized by many authors (e.g., Seehafer, 1996; Choudhury, 2003) that the signs of magnetic helicity should be opposite in small scales (fluctuating field) and large scales (mean field), yet it is unknown whether the current helicity observed from photospheric vector magnetic field (e.g., Bao & Zhang, 1998) reflect the characteristic scale of small or large. We also do not know which scale our measurements of kinetic helicity represents, therefore, it is perhaps inappropriate to conclude that the kinetic helicity from our measurements has an opposite sign with the current (or magnetic) helicity observed by many previous authors. On the other hand, the conventional sign of kinetic helicity in the bulk of the convection zone in the northern hemisphere is negative (Moffatt, 1978), as observed by time-distance helioseismology study on the global scale (Duvall & Gizon, 2000). But Rüdiger, Pipin, & Belvedère (2001) argued the kinetic helicity should be positive for the compressible magnetized plasma where magnetic helicity plays an important role. The preponderance of the positive kinetic helicity in the northern hemisphere in our statistics may support this argument.

Another interesting result from our statistical study is that the mean magnetic strength in the active regions is roughly proportional to the mean magnitude of the z-component of kinetic helicity. It is generally believed that the solar poloidal magnetic field is produced by the α-effect, and numerical simulations (Brandenburg, Saar, & Turpin, 1998) have showed that $\langle \alpha_v \rangle$ could increase with the increase of $\langle \mathbf{B} \rangle$, although in some cases α-quenching would be present, viz $\langle \alpha_v \rangle$ decreases with the increase of $\langle \mathbf{B} \rangle$. The observation that $\langle \alpha_v \rangle$ is proportional to $\langle \mathbf{B} \rangle$ may show us that the mean magnetic field in the solar active regions is much smaller than the equipartition magnetic strength, thus too weak to provoke the α-quenching effect. In addition, the average of the magnetic fields may have smeared out the α-quenching effect in some strong magnetic strength areas. Once again, we understand that the α-effect may mainly work in the bulk and bottom of the convection zone rather than near the solar surface, therefore more studies of the dynamics in the whole convection zone are required to better understand the formation of magnetic fields in active regions. Nonetheless, the present study in the active regions in the upper convection zone should provide some valuable observational evidence to understand the α-effect of solar dynamo theory.